Journal of Materials Chemistry

Cite this: J. Mater. Chem., 2011, 21, 11605

www.rsc.org/materials

PAPER

Ligands affect the crystal structure and photovoltaic performance of thin films of PbSe quantum dots†

Chih-Yin Kuo,[a] Ming-Shin Su,[a] Ching-Shun Ku,[b] Shu-Min Wang,[a] Hsin-Yi Lee[b] and Kung-Hwa Wei*[a]

Received 16th December 2010, Accepted 2nd February 2011
DOI: 10.1039/c0jm04417b

We have prepared thin films of PbSe quantum dots (QDs) featuring three different ligands, oleic acid (OA), butylamine (BA), and 1,2-ethanedithiol (EDT), which have pronounced affects on the arrangement and photovoltaic performance of the PbSe QDs in the thin films. Transmission electron microscopy revealed that ligands that altered the inter-QD spacing induced significant changes in the packing of the PbSe QDs in localized regions of small areas (300 × 300 nm) of the thin films: from a superlattice of OA-capped PbSe QDs to a chaotic pattern of EDT-capped PbSe QDs. Using a synchrotron X-ray reflectivity probe and data fitting, we determined that the roughness decreased and the average densities increased for large-area (1.5 × 1.5 cm) PbSe QD thin films capped with BA and EDT, relative to those of the OA-capped PbSe QD film. In particular, the PbSe QDs' vertical packing density, which is critical for charge transport, increased substantially for the system incorporating EDT ligands. As a result, devices containing the EDT-treated PbSe QD film as the active layer displayed much improved power conversion efficiencies (PCEs) relative to those of corresponding devices featuring either the OA- or BA-capped PbSe QD films as active layers. Adopting a layer-by-layer technique, we fabricated a EDT-capped PbSe QD device that exhibited a PCE of 2.45%.

Introduction

Solution processing of conjugated polymers,[1–4] organic small molecules,[5,6] and colloidal quantum dots (QDs)[7–13] have many potential benefits, particularly for the rapid and cost-effective preparation of flexible, large-area photovoltaic devices. Solar cells made from polymers typically absorb at wavelengths up to 800 nm, even though the optimal single-junction bandgap of solar cells lies in the region of 1100 nm.[14] An important approach toward realizing significant improvements in performance involves extending the spectral sensitivity of cells to near-infrared wavelengths, which contain as much as half of the energy of the Sun's power spectrum. Such a system can potentially be achieved using Pb-salt colloidal QDs as light-harvesting materials, because their optical bandgap can be tuned to a desired range by virtue of the quantum size.[15–18] Moreover, colloidal Pb-salt QDs can potentially undergo multiple exciton generation,[19–21] the generation of more than one electron/hole pair, resulting in enhanced photocurrents, which thereby increase the AM1.5 power conversion efficiency (PCE).[22–24]

The development of Pb-salt colloidal QDs for use in solar cells has undergone rapid advances, becoming a particularly active area of investigation. For example, a PbS QD solar cell featuring a strongly bound bidentate ligand to passivate the PbS QDs, developed through a solution exchange process, has exhibited an AM1.5 G PCE of 3.6%.[25] Solar cells based on PbSe QD films formed using a layer-by-layer (LBL) technique have exhibited AM1.5 G PCEs of 2.1–2.4%.[26,27] Solar cells based on highly confined ternary PbS_xSe_{1-x} QDs have provided a 3.3% AM1.5 G PCE.[28] Moreover, large improvements in PCEs have been obtained when combining Pb-salt QDs with metal oxide (TiO_2 and ZnO) heterojunctions.[29–33]

The surfaces of colloidal QDs typically possess long-chain and electrically insulating organic ligands, which must be shortened or removed for use in optoelectronic device applications.[34,35] A major challenge of current research into colloidal QDs is to devise methods for ligand exchange or chemical treatment with shorter molecules to reduce the inter-QD spacing and, thereby, create more-conductive QD films. Although some studies have been performed in this direction,[36,37] the influence of ligands on the detailed structure of QD thin films—for example, how the QDs are packed in different directions or the roughness and density of their packing—has never been explored. Structural information relating to QD films is not only of scientific interest; it also provides insight into how the QD films perform as active layers in photovoltaic devices. For example, one of the challenges

[a]Department of Materials Science and Engineering, National Chiao Tung University, 1001 Ta Hsueh Road, Hsinchu, 30050 Taiwan, ROC. E-mail: khwei@mail.nctu.edu.tw; Fax: +886 35 724727; Tel: +886 35 731871
[b]National Synchrotron Radiation Research Center, 101 Hsin-Ann Road, Science-Based Industrial Park, Hsinchu, 30077 Taiwan, ROC

† Electronic Supplementary Information (ESI) available: SEM and TEM images of various PbSe QDs; GIXRD patterns of PbSe QDs films on different substrates; XRR fitted parameters. See DOI: 10.1039/c0jm04417b/

that must be overcome if we are to employ colloidal QDs in photovoltaic devices is the poor charge transport properties of neat QD films. Rationally achieving this goal requires a deep understanding of the optical, structural, and electronic properties of QD films.

In this study, we investigated the effects of three different ligands—oleic acid (OA), butylamine (BA), and 1,2-ethanedithiol (EDT)—on the structures and photovoltaic performances of PbSe QD films. We used Fourier transform infrared (FTIR) spectroscopy, transmission electron microscopy (TEM), X-ray photoelectron spectroscopy (XPS), and synchrotron grazing incidence X-ray diffraction (GIXRD) to probe the structures of PbSe QDs films capped with these ligands. Additionally, we measured the current density–voltage characteristics of devices containing these ligand-capped PbSe QD films as active layers to compare their photovoltaic performance. We first synthesized OA-capped PbSe QDs in toluene, precipitating them using centrifugal force. We then added anhydrous BA to perform ligand exchange on the PbSe QDs in solution, again using centrifugal force to obtain BA–PbSe QDs. Suspensions of both the OA- and BA–PbSe QDs in octane were then spin-coated as films onto various substrates for further characterization. Soaking the BA–PbSe QDs films on substrates in EDT solution for a short period of time provided EDT–PbSe QD films. Scheme 1 depicts the procedure we used to prepare the PbSe QD films.

Experimental methods

Materials

Lead(II) oxide (PbO, 99.9%), selenium (Se, 99.9%), OA (tech. 90%), trioctylphosphine (TOP, tech. 90%), 1-octadecene (ODE, tech. 90%), and BA (99.5%) were purchased from Sigma–Aldrich. EDT (>98%) was acquired from Fluka. Anhydrous octane, MeCN, MeOH, toluene, isopropanol, and tetrachloroethylene (TCE, 99.9%) were obtained from J. T. Baker.

PbSe QDs[38]

PbO (0.8920 g, 4.00 mmol) was dissolved in a mixture of OA (2.825 g, 10.00 mmol) and ODE (12.83 g) in a three-necked flask and heated at 165 °C under vigorous stirring and a continuous Ar flow for 45 min to obtain a colorless, clear solution. At this temperature, 10% Se-TOP solution (6.4 g) was rapidly injected into the solution, dropping the temperature to *ca.* 150 °C for the growth process. Typically, 4.5 nm colloidal QDs were obtained after allowing the reaction to proceed for 45 s; cold toluene was injected into the mixture to terminate the reaction. The colloidal QDs were subsequently isolated from the growth mixture through repeated precipitation with MeOH prior to dispersal in toluene to remove any excess of unreacted ligands.

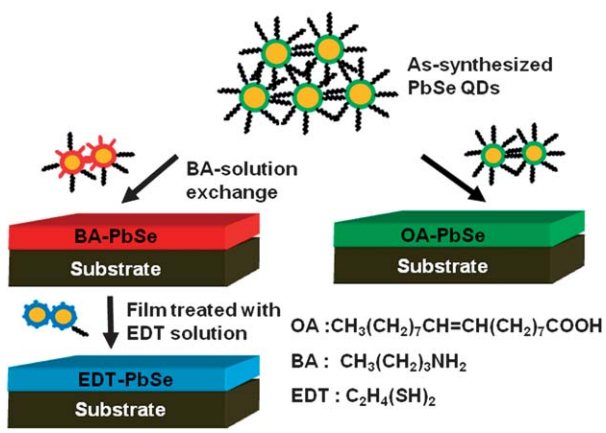

Scheme 1 Fabrication of PbSe QD thin films incorporating various ligands.

BA solution ligand exchange[39]

The as-synthesized PbSe colloidal QDs were redispersed in anhydrous BA solution and stirred continuously for 48 h in a N_2-filled glove box. The BA-exchanged QDs were precipitated with anhydrous isopropanol, dried, and redispersed in anhydrous octane.

QD films

All processing was performed in a N_2-filled glove box. PbSe colloidal QDs were spin-coated from octane (80 mg mL^{-1}) onto various substrates, including polished Si substrates, indium tin oxide (ITO), and copper grids fixed on glass substrates. The BA-exchanged QDs films were then soaked in a 1 mM EDT in MeCN for several seconds before being rinsed with anhydrous MeCN to remove any residual free-standing EDT.

Material characterization

Attenuated total reflection Fourier transform infrared (ATR-FTIR) spectra were recorded at room temperature using a Perkin–Elmer Spectrum100 spectrometer. Optical absorption data were acquired using a Hitachi U-4100 spectrophotometer equipped with an integrating sphere. XPS was performed using a Thermo VG Scientific Microlab 350 instrument, monochromated Mg Kα radiation, and a pass energy of 29 eV. TEM images were recorded using an FEI Spirit TWIN instrument operated at 120 keV. The surface normal wide-angle X-ray scattering (WAXS) and in-plane GIXRD measurements at high resolution were performed at the wiggler beamline BL-17B1 using an eight-circle diffractometer in the National Synchrotron Radiation Research Center (NSRRC), Hsinchu, Taiwan. For GIXRD and WAXS analyses, the photon energy was 8 keV with a flux estimated to be 10^{11} photons s^{-1}. Use of two pairs of slits between the sample and the detector provided a typical wave-vector resolution of *ca.* 0.001 nm^{-1} in the vertical scattering plane in this experiment.

Device fabrication and characterization

The patterned ITO on the glass substrate (5 Ω $sq.^{-1}$, Merck) was cleaned through sequential ultrasonic treatment with detergent, MeOH, acetone, and isopropanol and then dried under a flow of N_2. Poly(3,4-ethylenedioxythiophene):poly(styrene sulfonate) (PEDOT:PSS; Baytron P VP AI 4083) was then spin-coated on the UV ozone–treated ITO; the sample was annealed at 150 °C for 1 h before being transferred to a N_2-filled glove box. For the OA-capped and BA-exchanged PbSe QD devices, the QDs in octane were spin-coated on the PEDOT:PSS layer that had

previously been deposited on the ITO electrode. For the EDT-treated QD device, the BA-exchanged QD film on the ITO electrode was soaked in 1 mM EDT for 5 s. Moreover, using the LBL technique, the BA-exchanged QD solution (50 mg mL^{-1}) was spin-coated on the PEDOT:PSS/ITO substrate and then the whole sample was treated with 1 mM EDT, rinsed with anhydrous MeCN and octane, and dried under a stream of N_2; these steps were repeated for four cycles. All the active layers were typically 120 ± 20 nm thick, as measured using a Veeco Dektak profilometer. Finally, 20-nm Ca and 100-nm Al top electrodes were deposited onto all of the samples at *ca.* 10^{-7} torr by thermal evaporation through a shadow mask. Four devices were fabricated on each substrate, each with an active area of 0.04 cm^2.

Current density–voltage characteristics of the PbSe QD devices were measured by illuminating these devices through a mask that fits[40] the electrode crossing area under simulated AM1.5 G irradiation (100 mW cm^{-2}) using a Xe lamp–based Newport 66902 150 W solar simulator equipped with a Keithley 2400 source measurement unit. For solar cell measurements, the spectrum of the solar simulator was calibrated as follows:[41] A PV-measurement (PVM-154) mono-Si solar cell (NREL calibrated) and a Si photo diode (Hamamatsu S1133) were used to check the irradiation of the exposed area (100 mW cm^{-2}). A mismatch factor (M = 1.34) was obtained when using the PVM-154 cell as the reference cell and the fabricated devices as test cells and recording spectra from 300 to 900 nm at intervals of 10 nm. The PVM-154 cell was combined with a KG-5 filter (350–700 nm passed, Newport) to simulate a reference solar cell having spectral responsivity from 350 to 700 nm. The calibration was based on the IEC-69094-1 spectrum. External quantum efficiency (EQE) data were recorded with respect to the Optosolar SPF50 spectrum response. A Si reference cell was used to calibrate the wavelengths of light from 300 to 1060 nm; a Ge reference cell, from 1060 to 1800 nm.

Results and discussion

Fig. 1a presents FTIR spectra of PbSe QD films that had experienced treatment with the different ligands; these spectra confirm the nature of the chemical species on the surfaces of the PbSe QD films. We subjected the films, of the OA-capped PbSe QDs, to two different ligand treatment processes: (i) BA-exchange and (ii) BA-exchange with subsequent EDT treatment. The presence of signals for COO^- stretching at 1400 and 1530 cm^{-1} in the FTIR spectrum of the BA-capped QD film indicates that some of the OA units had been removed; a comparison of the area under the COO^- stretching region in the FTIR spectrum of the OA-capped PbSe QDs to that of the BA-exchanged PbSe QD film reveals that 14% of the OA ligands had been removed during the mixing process in anhydrous BA. The spectrum of the BA-exchanged QD film features a weak signal in the range 3250–3400 cm^{-1}, indicating the presence of amino groups. This BA ligand exchange on the PbSe QDs, albeit only partially completed, was designed to improve the quality of subsequently spin-coated PbSe QD films by reducing the domain boundaries in the PbSe QDs films, resulting in a smoother BA-exchanged PbSe QD film relative to that of the initially prepared oleate-capped PbSe QDs (*cf.* Figures S1a and S1c, ESI†). Moreover, the intensities of the signals for both the COO^- and

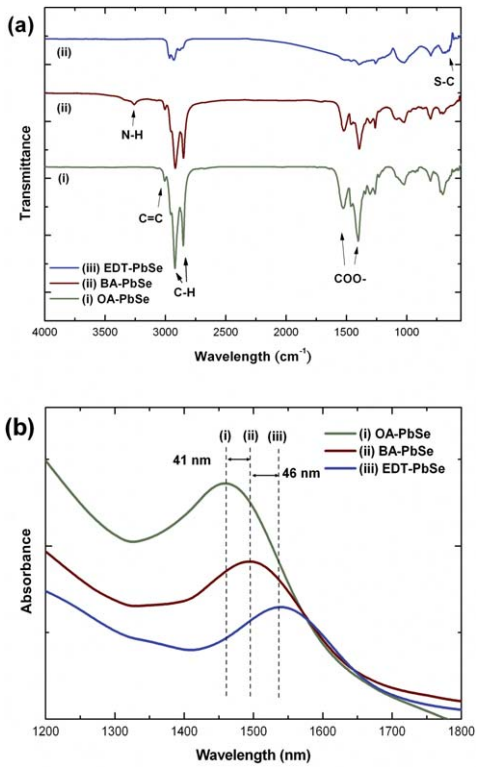

Fig. 1 (a) ATR-FTIR spectra and (b) optical absorption spectra of PbSe QD films capped with (i) OA, (ii) BA, and (iii) EDT, prepared through spin-coating onto substrates. Average size of PbSe QDs: 4.6 nm.

C–H units were dramatically reduced in the spectrum of the EDT-treated PbSe QD film, indicating that most of the OA ligands on the PbSe QDs had been exchanged, because thiol–Pb bonds are much stronger than amine–Pb or carboxyl–Pb bonds.[42] Further evidence to support this argument was provided by the appearance of a signal for the S–C bonds of the EDT ligands at 650–680 cm^{-1} in the spectrum.

Fig. 1b displays absorption spectra of the PbSe QD films capped with the various ligands. The first exciton absorption peak of OA-capped QD film was located at 1455 nm; the average size of the PbS QDs was 4.6 nm, as estimated from the TEM image in Fig. S2 (ESI,†). Given that the absorption spectra of the PbSe QD films were similar to that of the PbSe QDs in tetrachloroethylene (data not shown), we can calculate the sizes of the PbSe QDs using eqn (1), which describes the dependence of a PbSe QDs' particle size on the position of its first absorption peak in solution:[43]

$$D = (\lambda - 143.75)/281.25 \quad (1)$$

where D (nm) is the average particle diameter of the PbSe QDs and λ (nm) is the first absorption peak position of the corresponding sample. The estimated size (4.6 nm) for the PbSe QDs is in good agreement with the diameter calculated (4.66 nm) for the PbSe QDs using eqn (1). Moreover, the BA-treated PbSe QD film and the PbSe QD film subsequently treated with EDT exhibited their first exciton absorption peaks at 1496 and 1542 nm, respectively. Thus, red-shifts of 41 and 87 nm, respectively, relative to the signal for the OA-capped QD film, imply higher

packing densities for the BA- and EDT-ligated PbSe QD films, presumably because of strengthened dipole–dipole interactions and cross-linking of the QDs, respectively. Such interactions reduce the inter-QD distances, in turn leading to increased PbSe QD packing densities and conductivities.[44]

We used XPS to detect the presence of elemental species on the surfaces of the PbSe QD films. Fig. 2a reveals a strong signal for oxygen atoms and a weak signal for carbon atoms at binding energies of 531 and 287.8 eV, respectively, in the spectrum of the OA-capped QD films; we assign them to the oxygen and carbon atoms of the carboxylate groups of OA units. Moreover, we assign a signal for carbon atoms at 284.7 eV to the alkyl chains of the OA units. The slight decreases in intensity of the signals for the oxygen and carbon atoms on the BA-exchanged QD film are consistent with the partial removal of OA ligand from the PbSe QD surface. The nitrogen atom spectrum of the BA-exchanged QD film features a signal at 399.1 eV, revealing the presence of the amino groups of the BA units. The simultaneous lack of signals for oxygen atoms and the decreased intensities of the signals for carbon atoms on the EDT-treated films are consistent with the fact that the OA ligands were removed. Moreover, the EDT-treated films revealed a signal for sulfur atoms at 161.8 eV, consistent with sulfur atoms bound to the PbSe QD surfaces as thiolate species.

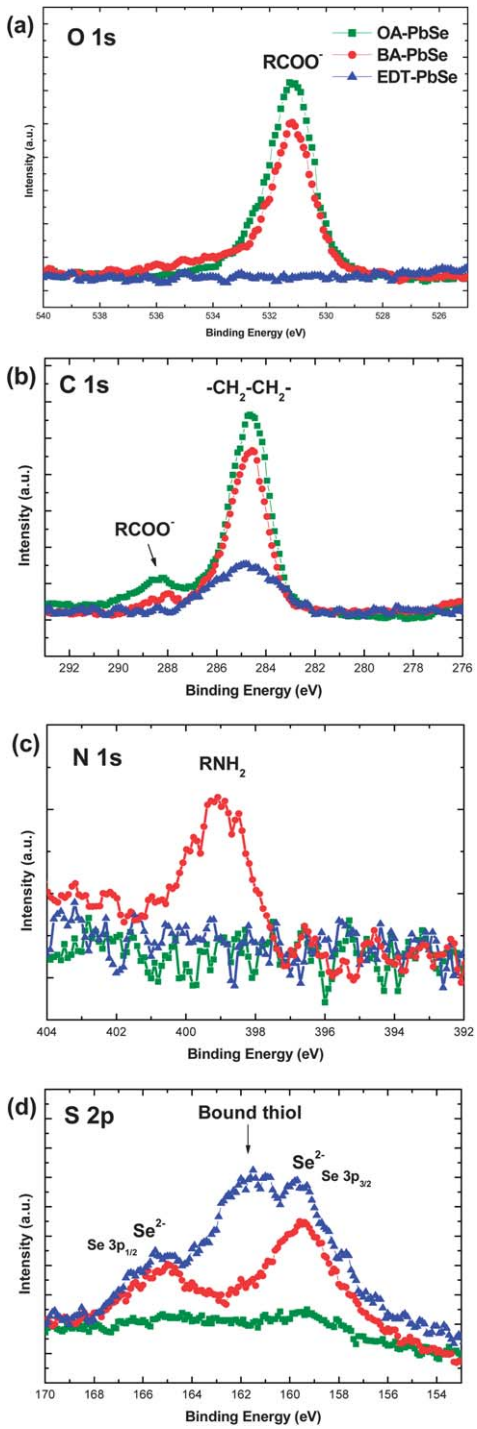

Fig. 2 XPS spectra of PbSe QD films capped with OA (squares), BA (circles), and EDT (triangles). The samples were spin-cast onto Si substrates and measured without exposure to air.

Fig. 3 displays TEM images, with (100) projections, of localized regions of the OA-capped, BA-exchanged, and EDT-treated PbSe QDs films. Fig. 3a presents the TEM image of the OA-capped film, revealing a large area of ordered PbSe QDs in a square assembly, exhibiting three-dimensional (3D) superlattices that had nucleated simultaneously and grown together on the Cu grids. The fast Fourier transform (FFT) image of the OA-PbSe QDs (inset to Fig. 3a) reveals a four-fold symmetry within the 3D ordered superlattice, consistent with the square assembly pattern of PbSe QDs in the TEM image. It has been reported that PbSe QDs form hexagonal assemblies when processed at a concentration of *ca.* 0.5–5.0 mg mL^{-1}.[45] We suspect that our large-area square assembly of QDs formed because we performed the spin-coating processing at a higher PbSe QD concentration. When we changed the concentration of the OA-treated PbSe QD solution or the film environment, the morphology of the film could become quite different; the TEM image in Fig. S5a (ESI,†), of a film obtained using a diluted PbSe QD solution (50 mg mL^{-1}), reveals a square assembly of PbSe QDs within the thicker region of the film, whereas the surrounding thinner region features a hexagonal assembly. Fig. S5b (ESI,†) presents TEM images of the film of the OA-capped PbSe QD superlattice after exposure to air; the QD superlattices transformed into a mostly hexagonal assemblies after exposure for 2 days. Fig. 3b displays a TEM micrograph of the BA-capped PbSe QDs, revealing some ordered and disordered domains, due to the partial removal of OA after BA solution exchange. Fig. 3c presents a TEM image of the EDT-treated PbSe QDs; this film featured a chaotic phase because of a loss of free volume during the EDT treatment process, leading to stress buildup and the formation of disordered domains, having an average size of *ca.* 100 nm, in the regions. The FFT image in the inset to Fig. 3c reveals vague square symmetry, indicating that the superlattice domain of the PbSe QDs film was destroyed and had become chaotic.

Fig. 4a presents synchrotron X-ray radial scans recorded along the surfaces normal to the spin-coated PbSe QD films capped with OA, BA, and EDT on Si substrates. The solid line is the fitted curve of the XRR part in the radial-scan data. Our simulation of the specular reflectivity, allowing us to acquire the physical parameters of the multilayer, was based on the recursive formalism of Parratt;[46] we then fitted the reflectivity data with the

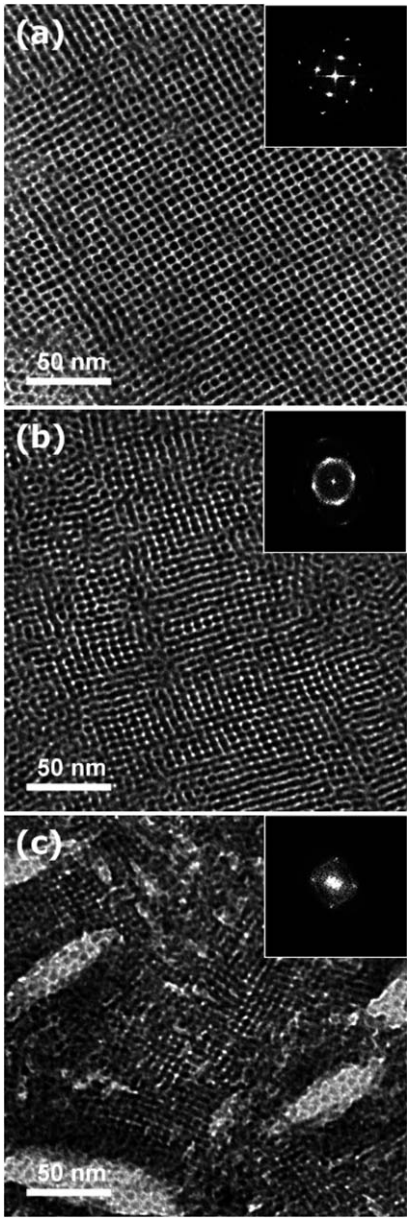

Fig. 3 TEM images of the 3D arranged superlattices of PbSe QDs films capped with (a) OA, (b) BA, and (c) EDT with (100) projections of lattices (scale: 50 nm). Insets: Corresponding FFT patterns revealing the ordering of the superlattices. The samples were prepared by spin-coating PbSe QD solutions (concentration: 80 mg mL^{-1}) onto Cu grids fixed on glass substrates under an inert atmosphere.

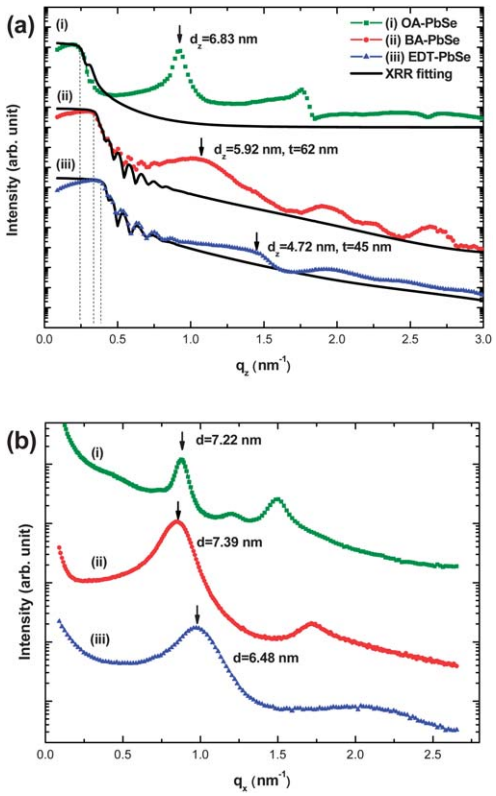

Fig. 4 Profiles of (a) the synchrotron X-ray radial scans along the surface normal and XRR fitting and (b) the in-plane CTR scans of (i) OA-, (ii) BA-, and (iii) EDT-capped PbSe QD films, prepared through spin-coating onto Si substrates (log-normal scale).

Bede$_{REFS}$ Mercury code[47] to determine the physical parameters of the multilayer, including its roughness, thickness, and density. Table S1 (ESI,†) lists the detailed XRR parameters. In Fig. 4a, the XRR fitting curves of the BA- and EDT-treated PbSe QD films exhibit more striking oscillations than that of the OA-capped PbSe QD film, providing direct evidence that treatment of the PbSe QDs with BA and EDT decreased the roughness of the films. From the fitted data, we obtained a roughness of 8.0 nm for the PbSe QD film capped with OA; this value was only 3.8 nm for both the BA-exchanged and EDT-treated PbSe QD films—almost a two-fold improvement with respect to that of the original QD film. Furthermore, the critical angle of total reflection, as indicated by the dashed line, increased substantially—implying increases in the average film density—after we treated the PbSe QDs with BA or EDT. The fitted densities for the OA-capped, BA-capped, and EDT-treated PbSe QD films were 1.86, 3.56, and 4.69 g cm^{-3}, respectively. Treatment of the BA-exchanged PbSe QD film with EDT caused the thickness of the resulting film to decrease from 62 to 45 nm, with an associated increase in the film density. In Fig. 4a, the first peaks, as indicated by the arrows and corresponding to the first-order Bragg diffraction from the films, shifted toward higher values of q when the PbSe QDs were treated with BA or EDT, revealing smaller inter-particle spacings in the packing directions along the surface normal of the films. Specifically, BA-exchange reduced the surface-normal d-spacing (d_z) from 6.83 to 5.92 nm, consistent with partial removal of the OA ligands. Treatment with EDT further removed most of the OA ligands and resulted in a surface-normal value of d_z of 4.72 nm, the largest decrease in all cases. The broadness of the first peaks of the BA-exchanged and EDT-treated films indicated that such chemical treatment destroyed the superlattice ordering of the OA-treated PbSe QD films as a result of the layers of PbSe QDs distorting during OA removal. Fig. 4b displays the X-ray in-plane crystal-truncation-rod (CTR) along the (H 0 0) direction. For the PbSe QD films capped with OA and BA, the d-spacings in the x direction were quite similar; the value of q_z was 0.87 nm^{-1} (d_x = 7.22 nm) for the former and 0.85 nm^{-1} (d_x = 7.39 nm) for the latter. For the PbSe

QD film capped with EDT, however, the values of the surface-normal d_z and in-plane d_x decreased to 4.72 and 6.48 nm, respectively, from 6.83 and 7.22 nm, respectively, for the OA-capped PbSe QD film.

Furthermore, the azimuthal scan (Phi scan) of these QDs films (Fig. S3, ESI†) all display fourfold symmetry, implying that the PbSe QD films maintained square assembled structures in the *ab* plane, consistent with the TEM results. Moreover, there was little difference between the in-plane CTR and azimuthal scans of the PbSe QD films when using either ITO/PEDOT:PSS or Si substrates (Fig. S4, ESI†); that is, there was no substrate effect on the structure of the PbSe QDs films. Table 1 lists the synchrotron X-ray characteristics of the PbSe QD films capped with OA, BA, and EDT.

Fig. 5 presents current density–voltage plots of the ligand-treated PbSe QD devices, each incorporating a thin PEDOT:PSS hole transport layer to improve the photovoltaic performance and stability.[27] The thickness of the active layer in each of these QD devices was 120 ± 20 nm, as measured using a profile-meter. The spin-casted OA-capped QD device exhibited very poor photovoltaic performance because of the low electrical conductivity of the 18-carbon-atom chains of the OA ligands (*ca.* 2 nm) on the PbSe QDs. For the BA-exchanged QD device, the short-circuit current density (J_{sc}), open-circuit voltage (V_{oc}), and fill factor (FF) were 1.58 mA cm^{-2}, 0.23 V, and 0.39, respectively. For the EDT-treated QD device, the values of J_{sc} and V_{oc} and the FF were 15.0 mA cm^{-2}, 0.16 V, and 0.37, respectively. As expected, the values of J_{sc} of the BA-exchanged and EDT-treated QD devices were significantly higher than that of the OA-capped PbSe QD device; indeed, the value of J_{sc} of the EDT-treated QD device was approximately nine times greater than that of the BA-exchanged QD device. The increase in the value of J_{sc} of the device incorporating the EDT-treated PbSe QD film resulted from this thiol-terminated cross-linker decreasing the interparticle spacing and increasing the film density; the decrease in V_{oc} was due to a decrease in the thickness of the QD film.

To further improve the photovoltaic performance of the PbSe QD devices, we optimized the device fabrication procedure using a LBL technique, with an intermediate BA ligand-exchange step in solution prior to EDT treatment of the films in the solid state. Fig. 6a displays the current density–voltage characteristics of a device incorporating a 110 ± 10 nm–thick layer of 4.6 nm-diameter PbSe QDs measured at room temperature in N_2-filled glove box under AM 1.5G conditions. The device exhibiting the highest performance—a maximum AM 1.5 G PCE of 2.45%—was prepared using four deposition cycles of PbSe QDs on an ITO/PEDOT:PSS substrate. Table 2 lists the photovoltaic performance parameters of these PbSe QD devices under solar illumination. Fig. 6b presents the EQE curve for best-performing PbSe QD device over the wavelength region from 300 to 1800 nm, covering the entire visible light range and a small portion of the near-infrared. The theoretical short-circuit current density, obtained after integrating the EQE curve, for this device was 23.6 mA cm^{-2}; this value is close to that (26.4 mA cm^{-2})

Table 1 Data from synchrotron X-ray radial scans along the surface normal and in-plane crystal-truncation-rod scans of the ligand-capped PbSe QD films. Average size of PbSe QDs: 4.6 nm

	OA–PbSe	BA–PbSe	EDT–PbSe
Thickness (nm)	140	62	45
Roughness (nm)	8	3.8	3.8
Average density of film (g cm^{-3})	1.86	3.56	4.69
Surface-normal *d*-space (nm)	6.83	5.92	4.72
In-plane *d*-space (nm)	7.22	7.39	6.48
Ordering of superlattice	good	poor	very poor

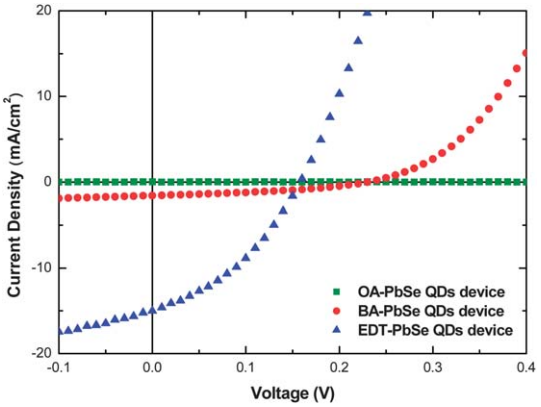

Fig. 5 Current–voltage characteristics of the ligand-capped PbSe QD devices on ITO/PEDOT:PSS substrates: OA-capped, BA-exchanged, and BA-exchanged with subsequent 1 mM EDT treatment for 5 s. The devices were illuminated under AM1.5 G conditions (100 mW cm^{-2}).

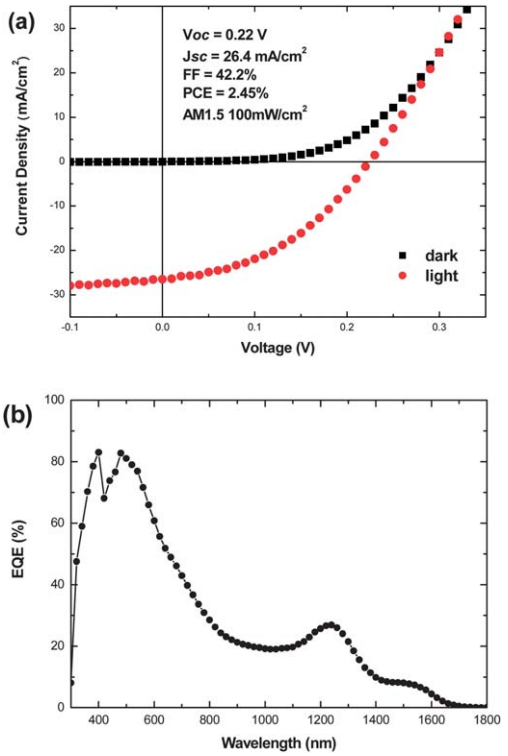

Fig. 6 (A) Current–voltage characteristics and (B) EQE spectrum of the EDT-capped PbSe QD device prepared on an ITO/PEDOT:PSS substrate using the LBL technique, under AM1.5 G irradiation (100 mW cm^{-2}).

Table 2 Photovoltaic parameters of PbSe QD devices measured under solar illumination. Device structure: ITO/PEDOT:PSS/PbSe QDs/Ca/Al

	V_{oc}[a] (V)	J_{sc}[b] (mA cm^{-2})	FF[c] (%)	η[d] (%)
OA-capped film	—	—	—	—
BA-exchanged film	0.23	1.58	39	0.14
EDT-treated film	0.16	15.0	37	0.89
EDT-treated film (LBL)	0.22	26.4	42	2.45

[a] V_{oc}: Open-circuit voltage. [b] J_{sc}: Short-circuit current density. [c] FF: Fill factor. [d] η: PCE. Solar: AM1.5 G (100 mW cm^{-2}).

obtained directly from the *I–V* curves, confirming the accuracy of our measurements.

Conclusions

The ligands OA, BA, and EDT affect the assembly and photovoltaic performance of PbSe QDs deposited in the form of thin films. Changes in the interparticle spacing induced by these ligands significantly influenced the ordering of the PbSe QD films, from superlattices to chaotic patterns. For PbSe QD films capped with BA and EDT, the roughness decreased and the average density increased relative to those of the OA-capped PbSe QD film. In particular, the vertical packing of the PbSe QDs, critical for charge transport, increased substantially after treatment with EDT. As a result, the PCE of a device containing the EDT-treated PbSe QD film as the active layer was much greater than that of the corresponding OA-capped PbSe QD device. Moreover, applying an LBL fabrication technique enhanced the PCE of a PbSe QD device to 2.45%.

Abbreviations

QDs	quantum dots
OA	oleic acid
BA	butylamine
EDT	1,2-ethanedithiol
PCEs	power conversion efficiencies
LBL	layer-by-layer
FTIR	Fourier transform infrared
TEM	transmission electron microscopy
XPS	X-ray photoelectron spectroscopy
GIXRD	grazing incidence X-ray diffraction
PbO	lead(II) oxide
Se	selenium
TOP	trioctylphosphine
ODE	1-octadecene
TCE	tetrachloroethylene
ITO	indium tin oxide
ATR-FTIR	attenuated total reflection Fourier transform infrared
WAXS	wide-angle X-ray scattering
PEDOT:PSS	Poly(3,4-ethylenedioxythiophene):poly (styrene sulfonate)
EQE	external quantum efficiency
3D	three-dimensional
FFT	fast Fourier transform
CTR	crystal-truncation-rod
J_{sc}	short-circuit current density
V_{oc}	open-circuit voltage
FF	fill factor.

Acknowledgements

This study was supported financially by the National Science Council of Taiwan (NSC 99-2120-M-009-003) and the U.S. Air Force Office of Scientific Research (AOARD-094039).

References

1 J. Y. Kim, K. Lee, N. E. Coates, D. Moses, T. Q. Nguyen, M. Dante and A. J. Heeger, *Science*, 2007, **317**, 222–225.
2 H. Y. Chen, J. Hou, S. Zhang, Y. Liang, G. Yang, Y. Yang, L. Yu, Y. Wu and G. Li, *Nat. Photonics*, 2009, **3**, 649–653.
3 W. J. E. Beek, M. M. Wienk and R. A. J. Janssen, *J. Mater. Chem.*, 2005, **15**, 2985–2988.
4 J. C. Hindson, B. Ulgut, R. H. Friend, N. C. Greenham, B. Norder, A. Kotlewski and T. J. Dingemans, *J. Mater. Chem.*, 2010, **20**, 937–944.
5 P. Peumans, S. Uchida and S. R. Forrest, *Nature*, 2003, **425**, 158–162.
6 F. Odobel, E. Blart, M. Lagrée, M. Villieras, H. Boujtita, N. El Murr, S. Caramori and C. Alberto Bignozzi, *J. Mater. Chem.*, 2003, **13**, 502–510.
7 S. A. McDonald, G. Konstantatos, S. Zhang, P. W. Cyr, E. J. D. Klem, L. Levina and E. H. Sargent, *Nat. Mater.*, 2005, **4**, 138–142.
8 W. A. Tisdale, K. J. Williams, B. A. Timp, D. J. Norris, E. S. Aydil and X. Y. Zhu, *Science*, 2010, **328**, 1543–1547.
9 I. Gur, N. A. Fromer, M. L. Geier and A. P. Alivisatos, *Science*, 2005, **310**, 462–465.
10 M. T. Zin, A. M. Munro, M. Gungormus, N. Y. Wong, H. Ma, C. Tamerler, D. S. Ginger, M. Sarikaya and A. K.-Y. Jen, *J. Mater. Chem.*, 2007, **17**, 866–872.
11 M. Law, J. M. Luther, Q. Song, B. K. Hughes, C. L. Perkins and A. J. Nozik, *J. Am. Chem. Soc.*, 2008, **130**, 5974–5985.
12 A. Kongkanand, K. Tvrdy, K. Takechi, M. Kuno and P. V. Kamat, *J. Am. Chem. Soc.*, 2008, **130**, 4007–4015.
13 B. Sun and N. C. Greenham, *Phys. Chem. Chem. Phys.*, 2006, **8**, 3557–3560.
14 C. H. Henry, *J. Appl. Phys.*, 1980, **51**, 4494–4500.
15 K. R. Choudhury, Y. Sahoo, T. Y. Ohulchanskyy and P. N. Prasad, *Appl. Phys. Lett.*, 2005, **87**, 073110.
16 K. Szendrei, W. Gomulya, M. Yarema, W. Heiss and M. A. Loi, *Appl. Phys. Lett.*, 2010, **97**, 203501.
17 K. R. Choudhury, D. W. Song and F. So, *Org. Electron.*, 2010, **11**, 23–28.
18 M. A. Hines and G. D. Scholes, *Adv. Mater.*, 2003, **15**, 1844–1849.
19 V. Sukhovatkin, S. Hinds, L. Brzozowski and E. H. Sargent, *Science*, 2009, **324**, 1542–1544.
20 M. C. Beard, A. G. Midgett, M. Law, O. E. Semonin, R. J. Ellingson and A. J. Nozik, *Nano Lett.*, 2009, **9**, 836–845.
21 M. Ji, S. Park, S. T. Connor, T. Mokari, Y. Cui and K. J. Gaffney, *Nano Lett.*, 2009, **9**, 1217–1222.
22 R. D. Schaller and V. I. Klimov, *Phys. Rev. Lett.*, 2004, **92**, 186601.
23 J. Tang, X. Wang, L. Brzozowski, D. A. R. Barkhosue, R. Debnath, L. Levina and E. H. Sargent, *Adv. Mater.*, 2010, **22**, 1–5.
24 N. Cho, K. R. Choudhury, R. B. Thapa, Y. Sahoo, T. Ohulchanskyy, A. N. Cartwright, K. S. Lee and P. N. Prasad, *Adv. Mater.*, 2007, **19**, 232–236.
25 R. Debnath, J. Tang, D. A. Barkhouse, X. Wang, A. G. Pattantyus-Abraham, L. Brzozowski, L. Levina and E. H. Sargent, *J. Am. Chem. Soc.*, 2010, **132**, 5952–5953.
26 J. M. Luther, M. Law, M. C. Beard, Q. Song, M. O. Reese, R. J. Ellingson and A. J. Nozik, *Nano Lett.*, 2008, **8**, 3488–3492.
27 C. Y. Kuo, M. S. Su, Y. C. Hsu, H. N. Lin and K. H. Wei, *Adv. Funct. Mater.*, 2010, **20**, 3555–3560.
28 W. Ma, J. M. Luther, H. Zheng, Y. Wu and A. P. Alivisatos, *Nano Lett.*, 2009, **9**, 1699–1703.

29 J. M. Luther, J. Gao, M. T. Lloyd, O. E. Semonin, M. C. Beard and A. J. Nozik, *Adv. Mater.*, 2010, **22**, 3704–3707.
30 A. G. Pattantyus-Abraham, I. J. Kramer, A. R. Barkhouse, X. Wang, G. Konstantatos, R. Debnath, L. Levina, I. Raabe, M. K. Nazeeruddin, M. Grätzel and E. H. Sargent, *ACS Nano*, 2010, **4**, 3374–3380.
31 J. J. Choi, Y. F. Lim, M. B. Santiago-Berrios, M. Oh, B. R. Hyun, L. Sun, A. C. Bartnik, A. Goedhart, G. G. Malliaras, H. D. Abruña, F. W. Wise and T. Hanrath, *Nano Lett.*, 2009, **9**, 3749–3755.
32 K. S. Leschkies, T. J. Beatty, M. S. Kang, D. J. Norris and E. S. Aydil, *ACS Nano*, 2008, **3**, 3638–3648.
33 T. Ju, R. L. Graham, G. Zhai, Y. W. Rodriguez, A. J. Breeze, L. Yang, G. B. Alers and S. A. Carter, *Appl. Phys. Lett.*, 2010, **97**, 043106.
34 D. V. Talapin and C. B. Murray, *Science*, 2005, **310**, 86–89.
35 Y. Liu, M. Gibbs, J. Puthussery, S. Gaik, R. Ihly, H. W. Hillhouse and M. Law, *Nano Lett.*, 2010, **10**, 1960–1969.
36 M. V. Kovalenko, M. Scheele and D. V. Talapin, *Science*, 2009, **324**, 1417–1420.
37 K. Szendrei, D. Jarzab, M. Yarema, M. Sytnyk, S. Pichler, J. C. Hummelen, W. Heiss and M. A. Loi, *J. Mater. Chem.*, 2010, **20**, 8470–8473.
38 W. W. Yu, J. C. Falkner, B. S. Shih and V. L. Colvin, *Chem. Mater.*, 2004, **16**, 3318–3322.
39 G. Konstantatos, I. Howard, A. Fischer, S. Hoogland, J. Clifford, E. Klem, L. Levina and E. H. Sargent, *Nature*, 2006, **442**, 180–183.
40 A. Cravino, P. Schilinsky and C. J. Brabec, *Adv. Funct. Mater.*, 2007, **17**, 3906–3910.
41 M. Y. Chiu, U. S. Jeng, C. H. Su, K. S. Liang and K. H. Wei, *Adv. Mater.*, 2008, **20**, 2573–2578.
42 M. V. Kovalenko, D. V. Talapin, M. A. Loi, F. Cordella, G. Hesser, M. I. Bodnarchuk and W. Heiss, *Angew. Chem., Int. Ed.*, 2008, **47**, 3029–3033.
43 Q. Dai, Y. Wang, X. Li, Y. Zhang, D. J. Pellegrino, M. Zhao, B. Zou, J. Seo, Y. Wang and W. W. Yu, *ACS Nano*, 2009, **3**, 1518–1524.
44 G. Sarasqueta, K. R. Choudhury and F. So, *Chem. Mater.*, 2010, **22**, 3496–3501.
45 T. Hanrath, J. J. Choi and D. M. Smilgies, *ACS Nano*, 2009, **3**, 2975–2988.
46 L. G. Parratt, *Phys. Rev.*, 1954, **95**, 359–369.
47 D. K. Bowen and B. K. Tanner, *Nanotechnology*, 1993, **4**, 175–182.

